PAPER

Check for updates

Sialylated glycan-based impedimetric biosensing for the detection of *Vibrio cholerae* biomarkers in cell culture media

Hen Okshtein, [a] Israel Alshanski, [a] Raghavendra Kikkeri, *[b]
Shlomo Yitzchaik *[a] and Mattan Hurevich *[a]

Cholera is a severe infectious disease caused by *Vibrio cholerae*. The disease primarily spreads through contaminated food and water sources; it remains a significant global health concern. The pathogenesis of *Vibrio cholerae* is facilitated by the secreted neuraminidase, *Vibrio cholerae* neuraminidase (VCNA). This neuraminidase cleaves host cell surface sialic acids, which leads to bacterial colonization and infection progression. This study presents the development of a label-free VCNA biosensor based on electrochemical impedance spectroscopy. The biosensor relies on synthetic sialosides that form self-assembled monolayers on gold electrodes. The system demonstrated selective detection of VCNA activity through distinct impedance variations corresponding to the enzymatic cleavage of the sialoside substrates. The VCNA activity was evaluated under varying environmental conditions, including different media and pH values. This approach provides insights into developing robust biosensing platforms for bacterial detection, offering potential applications in various diagnostic and monitoring systems.

Introduction

Cholera disease is caused by the toxin of the *Vibrio cholerae* (VC) bacterium. The disease primarily spreads through contaminated food and water sources. Infection leads to severe acute intestinal infections, causing rapid dehydration and death if untreated.[1] Recent data highlights a surge in global cholera cases. In 2023 alone, over 535 000 cases and more than 4000 fatalities were reported across 45 countries, marking a 13% increase in cases and a 71% rise in deaths compared to 2022. This increase underscores the impact of factors like climate change, access to clean water, and sanitation in exacerbating outbreaks.[2] Early detection of VC in the food supply chain plays a key role in disease epidemiological prevention and management.[3]

The current gold standard methodologies for cholera diagnosis primarily rely on the isolation of VC from stool samples *via* selective media culture, a process that typically requires up to 8 days for conclusive confirmation.[4] While the polymerase chain reaction (PCR) is also recognized as a gold standard diagnostic technique for cholera, its widespread application is constrained by the prerequisite for a specially equipped laboratory environment,

comprehensive logistical support, and highly specialized personnel.[5,6] The enzyme-linked immunosorbent assay (ELISA) is a widely used method for disease detection, but the method has several downsides in glycan-related applications. The reliance on labelled reagents adds complexity, requires extensive sample preparation, and increases costs. Loop-mediated isothermal amplification (LAMP) offers rapid and cost-effective detection but faces challenges in maintaining reaction conditions, limiting its applicability.[4,7–9] The development of robust cholera detection methods for the whole food system value chain holds promise in overcoming these limitations.

Sialic acid (SA), a distinctive monosaccharide, exhibits structural characteristics that differentiate it from other glycans. SA is abundant in biological systems, at the terminal of glycosphingolipids, glycophosphoinositol anchors, and sialosides on the cell surface. Sialosides are *O*-glycans, *N*-glycans, and other SA-modified polyglycoconjugates.[10–12] Due to its unique physicochemical characteristics, SA is prominently found on the cell surface, where it plays a crucial role in mediating cellular recognition processes, modulating immune system responses, and participating in diverse intracellular signaling pathways.[10,13] The central role of SA in cell recognition and bacterial infection processes highlights its potential for diverse biosensing applications,[14,15] ranging from metabolic monitoring to disease detection.

Neuraminidases (NA), as exo-α-sialidases, represent a vital class of glycoside hydrolase enzymes. These enzymes, which

[a] *Institute of Chemistry and Center of Nanoscience and Nanotechnology, The Hebrew University of Jerusalem Givat Ram, Jerusalem, 91904, Israel.*
E-mail: mattan.hurevich@mail.huji.ac.il, shlomo.yitzchaik@mail.huji.ac.il
[b] *Indian Institute of Science Education 355 and Research, Pune 411008, India.*
E-mail: rkikkeri@iiserpune.ac.in

can exist in both secreted and membrane-bound forms, catalyze the hydrolysis of sialic acid residues from glycoconjugates on cell surfaces. Different NAs exhibit selective activity towards various sialosides, reflecting their precise roles in biological systems. Such enzymatic activity is integral to critical processes, including intricate host–pathogen interactions, bacterial virulence mechanisms, and microbial nutrition acquisition.[16,17]

Evaluating the enzymatic activity of NA against specific sialosides, utilizing diverse methodologies, represents a promising approach for sensitive and selective detection of bacterial and viral pathogens.

Vibrio cholerae neuraminidase (VCNA) is instrumental in bacterial adhesion and host–pathogen interactions, mediating pathogenesis processes such as toxin internalization through endocytosis. The detection and characterization of VCNA in biologically relevant environments and substrates pose considerable challenges. This can be attributed to the enzyme's sensitivity to various factors such as pH, ionic strength, and ion composition, all of which influence neuraminidase activity. Consequently, these physicochemical parameters modulate enzymatic function, thereby affecting host cell entry and metabolic interactions within mammalian systems. Labelled substrate assays, such as chromogenic, fluorogenic, and luminogenic methods, are widely used due to their high sensitivity, rapid readouts, and compatibility with high-throughput screening. Chromogenic assays utilize substrates that undergo color changes upon enzymatic cleavage, providing visual detection.[18,19] Fluorogenic assays based on employing fluorescent substrates and monitoring the change in fluorescence upon enzymatic modification provide sensitive and quantitative readouts.[20,21] Luminogenic assays rely on substrates that generate luminescent signals upon enzymatic reaction, offering rapid and sensitive detection.[22] Labelled substrate methods are susceptible to spectral interference from the tested inhibitors, and can lead to signal quenching or increased background fluorescence.[23] In contrast, label-free methods encompass chemical modification approaches, including thiobarbituric acid (TBA),[24] periodic acid-Schiff (PAS), and enzyme-linked lectin.

TBA assays measure the release of *N*-acetylneuraminic acid generated by NA, while PAS and enzyme-linked lectin assay (ELLA) lectin-based assays detect the cleavage of sialic acid residues on glycoproteins. These label-free techniques utilize natural substrates, enabling the determination of linkage-specific NA activity. However, they can be labour-intensive, require multistep procedures, may involve toxic reagents, and can be susceptible to interference from biological sample components.[25–28]

Electrochemical impedance spectroscopy (EIS) is a sensitive, label-free analytical technique for evaluating interfacial properties at the electrode surface. By applying an alternating current signal, EIS measures the impedance and alterations in the dielectric properties of the recognition layer. Impedance is the transfer function that comprises resistance and capacitance, corresponding with the systems response to an alternating current (AC) signal across a range of frequencies. The dielectric properties typically arise from the functionalization of the electrode surface and change due to specific analyte interactions. This method quantifies variations induced by enzymatic interactions with electrode-functionalized substrates, which is often achieved by monitoring the diffusion of a redox-active species through the recognition layer.[29–34] The enzymatic activity changes the substrate structure, which induces conformational changes at the sensor interface, thereby modulating its dielectric or electrochemical properties.[35,36] EIS is a widely used technique in biosensing applications, enabling the development of highly sensitive detection methods for a diverse range of analytes, from ions to bacteria. The high sensitivity and specificity of EIS-based biosensors make them invaluable tools for various applications, such as environmental monitoring,[37] medical diagnostics,[38–40] and food safety analysis.[41,42]

EIS is a highly versatile analytical technique with widespread applications across various fields, including its utility in the development of sensitive and selective biosensors through the analysis and immobilization of bio-recognition elements.

A common electrode in EIS-based biosensing is comprised of glassy carbon or gold. The recognition layer can be covalently bound to the different electrodes through various techniques to form self-assembled monolayers (SAMs).[43] Glassy carbon electrodes (GCEs) proved inadequate to follow enzymatic reactions on sialosides.[44] In that study, gold electrodes (AuEs) were selected for VCNA biosensor development as they proved to preserve NA catalytic activity. Therefore, the use of EIS combined with diverse glycans offers a label-free and sensitive method for biosensing applications such as monitoring the activity of neuraminidase and sialyltransferase and differentiating between NAs based on activity on sialoside with structural variation.[39,44–48]

In this study, we demonstrate the application of an EIS-based biosensor platform for VC bacterial detection, utilizing synthetic sialosides to target secreted VCNA. This study examines the effects of environmental factors such as pH and complex biological environments on enzyme activity and sensor performance. This approach provides a foundation for robust biosensor design for bacterial infection detection.

Experimental

Electrode surface modification

The **AuE** was modified manually, the electrode was polished using 0.05 μm alumina powder embedded in a microcloth (Buehler), then washed with triple distilled water (TDW) three times. After the polishing step, the electrode was modified with 1 mM α-lipoic acid (LPA):EtOH solution for 1 h at 25 °C, then rinsed with EtOH and TDW three times. The electrode was treated with a solution of 1 mg mL^{-1} of (1-cyano-2-ethoxy-2-oxoethylidenaminooxy)dimethylamino-morpholino-carbenium hexafluorophosphate (COMU):acetonitrile (ACN) and 1% *N,N*-diisopropylethylamine (DIPEA), incubated for 1 hour at 25 °C, then washed in ACN. The alkyl-amine terminated sialoside concentration was 2 μm in 0.2 mL TDW and incubated for 1 h at 37 °C. After the modification, the electrodes were rinsed with TDW and stabilized in 50 nM AB for 1 hour at 37 °C. The

enzyme solution was prepared according to the protocol described here. The modified electrodes were exposed to the enzyme for 1 hour at 37 °C.

Electrochemical measurements

The electrochemical impedance spectroscopy (EIS) measurements were performed in a standard three-electrode electrochemical cell setup. The AC potential source is provided by a BioLogic SAS SP-300 potentiostat under single sine AC excitation at a potential of 0.21 V with 10 mV amplitude in the frequency range from 100 kHz to 0.1 Hz. The electrochemical cell comprises a reference electrode Ag/AgCl, a working electrode (2 mm AuE), and a Pt billet as a counter electrode. The measurements were performed in $[Fe(CN)_6]^{3-}/[Fe(CN)_6]^{4-}$ 5 mM and KCl 100 mM solution, and 50 mM acetate buffer at pH 5. The experimental results were fitted to the Randel equivalent circuit represented as $R_S[(R_{CT}W)\|Q]$. R_S is the resistance of the solution, R_{CT} is the charge-transfer resistance of the layer, Q is the constant phase element, and W is the 120 Warburg diffusion element. The normalized R_{CT} is calculated as the ratio between the R_{CT} after and before the enzymatic exposure.

Exposure to the enzyme

Stock samples of NA were prepared as previously described.[47] Stock samples of NA were dissolved in 200 μL of 50 mM acetate buffer (AB) (pH 5.2). 2 μL of each stock solution was added to 178 μL of 50 mM AB, giving a final volume of 0.18 mL (3 mU

mL^{-1}). Each modified electrode was drop-cast with 60 μL of the solution for 1 hour at 37 °C. After the exposure, the electrodes were rinsed with TDW.

Results and discussion

Preparation of and characterization of the sialoside Au electrodes

The **Au**Es were modified with four different synthetic sialosides (Fig. 1). The four substrates share the same LacNAc core structure, while the SA structural variations allow for enzymatic regioselectivity. The differences between the sialosides arise from the presence of two distinct types of sialic acid and two variations in their glycosidic linkages. The first two substrates resemble human-type sialosides, with acetyl on C-5, namely, Neu5Ac, and either 2,6 or 2,3 connectivity (**H6**, **H3**). The other two substrates resembled non-human mammalian sialosides with hydroxy acetyl at position 5, namely, Neu5Gc with connectivity 2,6 (**M6**) and 2,3 (**M3**). The glycan assembly on **Au**Es was performed in a stepwise manner (Fig. 1) following the previously described protocol and is presented for **H3**. Polished **Au**Es were functionalized with LPA to provide **AuE-LPA** (Fig. 1, step I). Following this modification, we characterized the monolayer using EIS and X-ray photoelectron spectroscopy (XPS). The EIS analysis showed a 2 kΩ (Fig. 2(A)) increase in R_{CT} due to the **Au**E's surface modification with LPA. Additionally, the XPS data indicated a layer thickness of 9 Å, corresponding to the calculated length of
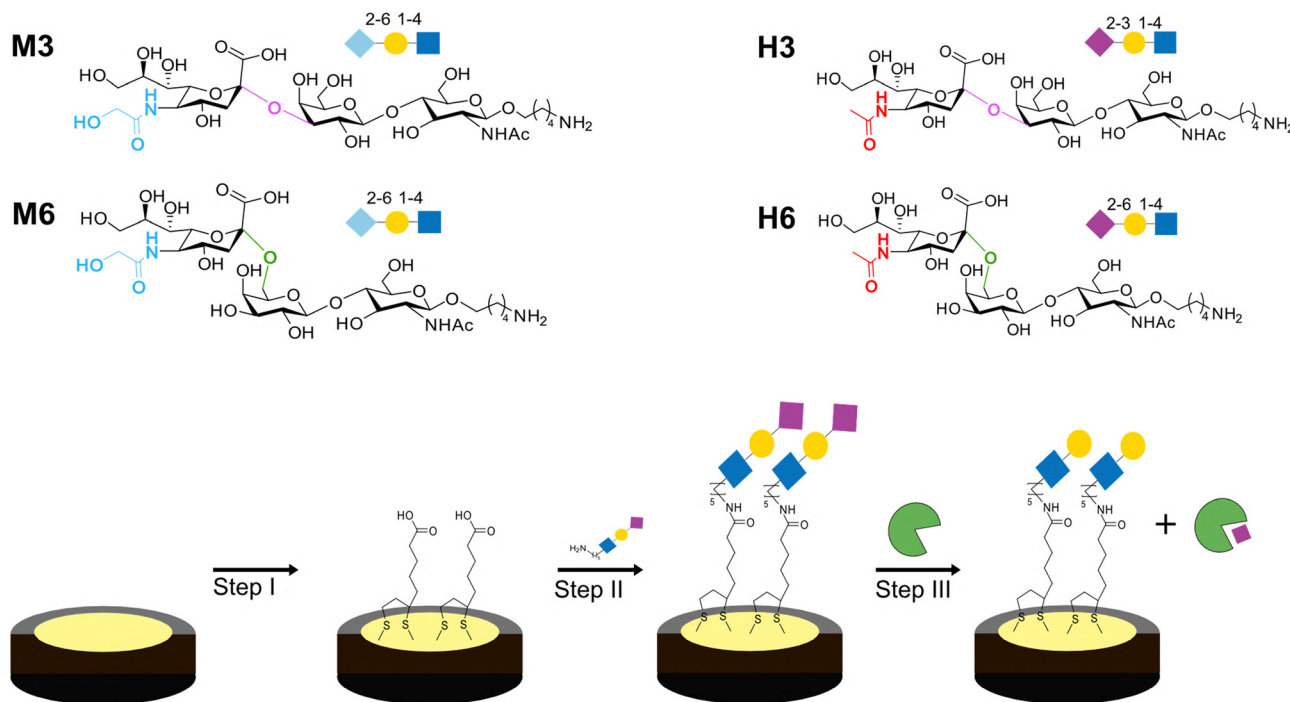

Fig. 1 The assembly of four sialosides on a gold electrode. Assembly steps: LPA self-assembly (step I), coupling the alkyl-amine terminated trisaccharide to the LPA (step II), exposure to VCNA (step III). The trisaccharides that were used in this study (top) with the structure and their corresponding symbol nomenclatures for glycan (SNFG): 2,6-Neu5Ac-Gal-GlcNAc trisaccharide (**H6**), 2,3-Neu5Ac Gal-GlcNAc trisaccharide (**H3**), 2,6-Neu5Gc-Gal-GlcNAc trisaccharide (**M6**), and 2,3-Neu5Gc-Gal-GlcNAc trisaccharide (**M3**). The **H3** and **H6** Neu5Ac acetyl is coloured red, and the **M3** and **M6** Neu5Gc glycolates are coloured blue. The 2–6 glycosidic bond is coloured green, and the 2–3 glycosidic bond is coloured magenta.

the LPA molecule. The LPA–trisaccharide coupling was achieved through an amidation reaction, wherein the amino group of the trisaccharide was coupled to the terminal carboxylic acid of the LPA using a 1-cyano-2-ethoxy-2-oxoethylidenaminoxy (COMU) coupling agent (Fig. 1, step II) to provide **AuE-H3**. The XPS analysis confirmed a 4 Å increase in the monolayer thickness, resulting in a total thickness of 13 Å. Support for modification of the LPA monolayer with the trisaccharides based on the polarization modulation reflection absorbance infrared spectroscopy analyses shows a distinctive peak for the C–N stretch at 1350 cm^{-1} (Fig. S3).

Additionally, the XPS data showed an enhanced signal in the N1s region, corresponding to the formation of the amide bond and the presence of the amide groups from the sialosides. The EIS analysis indicated an increase of 10 kΩ in the R_{CT}, and the change in R_{CT} is consistent with the modification of the LPA monolayer with the trisaccharide. The extent of monolayer modification with the trisaccharide **H3** was quantified *via* XPS by calculating the N/S atomic ratio. An increase in this ratio, resulting from the amidation of LPA terminal carboxylic acids with the sialoside, indicated that 43% of the SAM was modified with **H3**, resulting in a surface coverage of 6.9×10^{13} molecules per cm^2.

EIS analysis of sialoside-based VCNA preference and sensitivity range

VCNA is a well-characterized sialidase enzyme that catalyses the hydrolysis of α-ketosidic linkages between terminal sialic acid residues from the adjacent subterminal glycan in the glycoconjugates.[10] **AuE-H3** was exposed to VCNA in acetate buffer (AB) at a temperature of 37 °C (Fig. 1, step III). This step shows a reduction in the R_{CT} of 9 kΩ (Fig. 2(A)) which corresponds with the removal of the SA by VCNA. The results indicate that the modification of **AuE**'s surface with sialosides increased the resistance to charge transfer, leading to a change in impedance as R_{CT} increased. Enzymatic activity by VCNA and the subsequent removal of sialic acid residues facilitated electron transfer, causing a corresponding decrease in R_{CT}. XPS analysis after treatment with VCNA showed no significant

increase in surface thickness or N1s signal, suggesting that the enzyme did not adsorb to the surface.

These observations support the effectiveness and stability of the sialoside-functionalized electrode and align with parameters reported in previous studies.[44]

EIS analysis was conducted on **AuE**s modified with one of four distinct sialosides. In each experiment, the biosensor was modified with different sialosides, followed by exposure to *Vibrio cholerae* neuraminidase in an acetate-buffered saline solution (Fig. 1, step III). Based on previous studies,[49–52] and similar results reported in sialoside-based biosensing,[38,43,44] EIS analysis results showed that treatment of the sialylated electrodes with VCNA led to a decrease in R_{CT}. To evaluate the differences among the sialosides, the normalized response was calculated by the ratio between the R_{CT} before the exposure to the R_{CT} after the enzymatic activity (Fig. 2(B), normalized R_{CT}, NR_{CT}). These results suggest that the most efficient catalytic activity of VCNA was on the **H3**-modified **AuE**s. The lowest activity was observed with the **M6** substrate, indicating lower catalytic efficiency. This observation aligns with previous solution-based enzyme activity studies for VCNA.[51] To evaluate the biosensor sensitivity towards VCNA, **AuE-H3** was screened against 0.0003 up to 3.0 mU mL^{-1} enzyme concentration. Significant EIS response was observed between 0.3–3 mU mL^{-1}, demonstrating the sensitivity of the biosensor platform (Fig. 2(C)).

VCNA biosensing in complex media

VCNA represents a promising biomarker for the detection of *V. cholerae*, particularly for applications in the food supply chain and public health. Non-optimal pH and the presence of multiple components in the analysed sample can interfere with the biomarker recognition of the biosensor. The development of reliable *V. cholerae* biosensors necessitates a comprehensive evaluation of VCNA activity under biologically relevant conditions.[48] We systematically investigated the electrochemical impedimetric response of the VCNA **H3** biosensing platform in different environmental conditions, focusing on pH and media composition effects (Fig. 3). To accommodate the pH
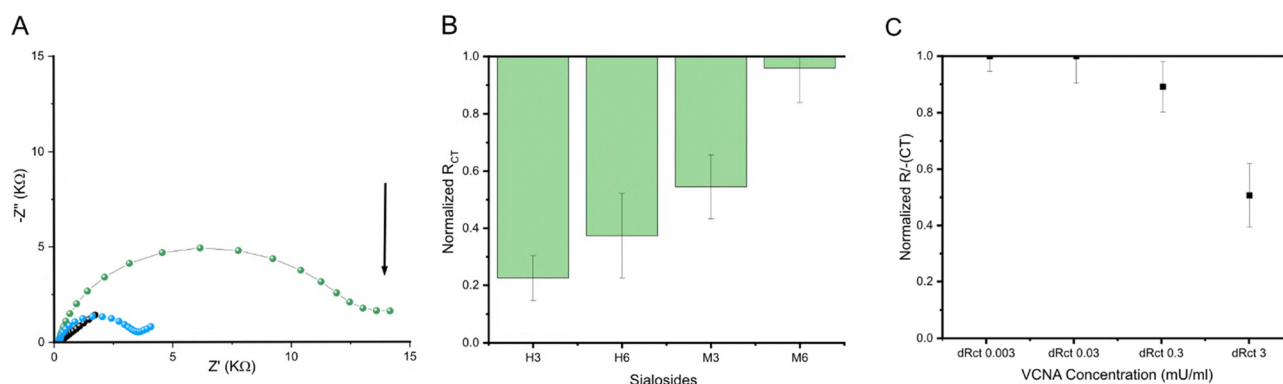

Fig. 2 (A) The Nyquist plots representing **AuE-H3** assembly and the VCNA response, bare **AuE** (black), **AuE-H3** substrate (green), and after exposure to VCNA in AB (teal); (B) the biosensor VCNA enzymatic activity toward different sialoside-modified **AuE**. The activity is represented as the normalized ratio of R_{CT} values, reflecting substrate-specific SA hydrolysis. (C) The biosensor limit of detection of the VCNA enzymatic activity toward **H3** sialoside-modified **AuE**. The error bar represents the standard deviation based on five repeats and the Nyquist plot is fitted with the equation $R_S[(R_{CT}W)\|Q]$.
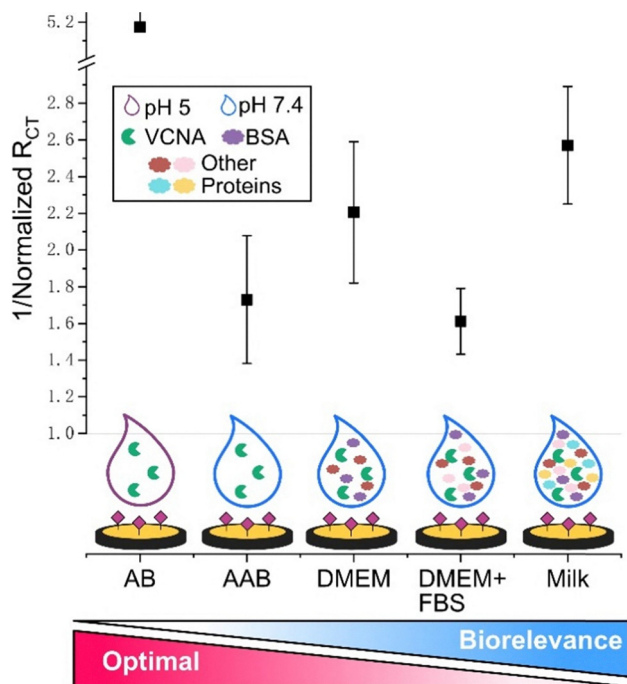
Fig. 3 Impedimetric response of the **AuE-H3** to VCNA conditions that vary from optimal (red) to biorelevant (blue). Response was measured in pH 5.0 (AB) or in pH 7.4 (AAB, DMEM, DMEM + FBS, milk). DMEM and DMEM + FSB represent two typical cell culture media that contain a large variety of proteins that might interfere with the biosensing. The normalized R_{CT} was calculated by dividing the response of the sialylated electrode by the response recorded after the exposure to VCNA.

variability inherent to food matrices, experimental parameters were adjusted accordingly. Initial studies were conducted in sterile AB at pH 5, representing optimal conditions for VCNA activity. To better simulate conditions relevant to food systems, impedimetric measurements of VCNA activity toward **H3** were subsequently performed in ammonium acetate buffer (AAB) at pH 7.4. Under these conditions, incubation of **AuE-H3** with VCNA in AAB resulted in a detectable decrease in impedance. The measured signal in AAB was less pronounced than in AB, and a clear and quantifiable impedimetric signal, consistent with enzymatic activity, was obtained at non-optimal pH.

To further evaluate the biosensor detection sensitivity in a more complex environment, studies were conducted in two typical cell culture media at pH 7.4. Biosensing was performed in either Dulbecco's modified Eagle medium (DMEM), which contains nutrients and proteins, or in DMEM supplemented with 10% fetal bovine serum (FBS). FBS is a vital supplement for cell culture media, providing essential components for cell growth and proliferation *in vitro*, namely high concentrations of proteins, a range of growth factors, nutrients, trace elements, electrolytes, and detoxifying agents, expanding the sensing environment complexity (Fig. 4). In both systems, a decrease in impedance was observed, indicating that VCNA was also active under these conditions. The impedimetric signal of those complex systems was comparable to the one observed under the simpler AAB system. In all three observed cases, there is a significant detectable signal for the enzymatic activity, proving
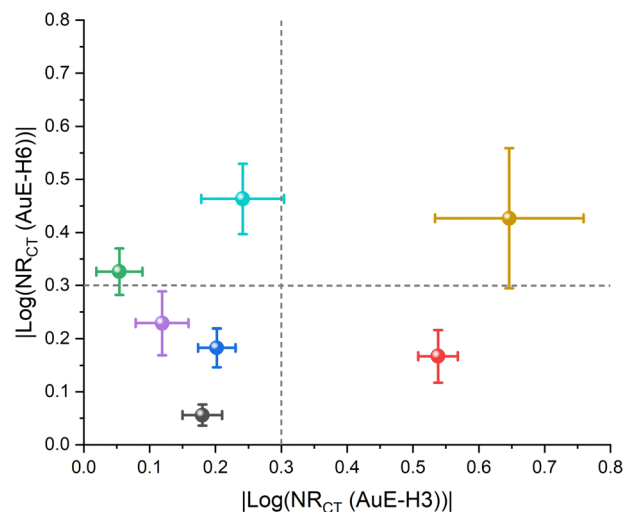

Fig. 4 Response of 3 mU mL^{-1} NAs from VC (brown), CP (blue), AU (green), SP (cyan), H1N1 (black), H3N2 (red), and H5N1 (purple) to **AuE-H3** and **AuE-H6**. The response was calculated by the equation of |log(normalized R_{CT})|. The error bar is based on five repeats.

that biosensing can be achieved even under non-optimal pH. These results indicate that the addition of cell growth media components does not impede VCNA activity. This suggests that the biosensor can be utilized in complex environments with a large number of components, such as cell growth media.

Extending the evaluation of the biosensor's performance in real-world applications, the activity of VCNA was subsequently measured in milk. This experiment aimed to assess the biosensor's robustness and applicability in a matrix highly relevant to food safety and public health, given that VC mainly spreads through contaminated food. While the complexity of the milk matrix, comprising a diverse array of proteins, lipids, and other macromolecules, could potentially interfere with enzymatic activity or sensor signalling, the impedimetric analysis supports VCNA detection. A slight increase in the normalized R_{CT} was observed, indicating that despite the non-optimal conditions and the intricate composition of milk, the biosensor maintained its ability to detect VCNA activity. This finding and the biosensor's functionality in cell culture media (DMEM and DMEM + FBS) show the biosensor's effectiveness under non-optimal pH and in the presence of various biological components.

VCNA biosensing fingerprints differ from other NAs

NA plays an important role as a virulence factor for numerous bacterial and viral pathogens. In previous works, we demonstrated that modified **AuE**s detect the activity of influenza neuraminidases, along with different bacterial NAs from *Arthrobacter ureafaciens* (AUNA), *Clostridium perfringens* (CPNA), and *Streptococcus pneumoniae* (SPNA).[39,44,53] The results indicate a degree of cross-reactivity in NA detection by a single sialoside. However, combining the responses of various NAs at the same concentration (3 mU mL^{-1}) and conditions (pH 5), utilizing **AuE-H3** and **AuE-H6**, yielded a distinguishable impedimetric pattern specific to *Vibrio cholerae* neuraminidase when compared to other NAs

(Fig. 4). The differential substrate preference can be attributed to two main factors. The first is the intrinsic kinetic preference of each NA, which is dictated by structural characteristics such as active-site architecture and catalytic pocket accessibility, in line with their biological function. For example, although both CPNA and VCNA are secreted NAs, and belong to the CBM40 lectin family, CPNA exhibits a shallower substrate-binding pocket, while VCNA possesses a broader cleft, which may confer greater flexibility in accommodating structurally diverse sialosides. This structural distinction is consistent with the higher activity observed for VCNA under the same assay conditions. The second factor involves interactions with the sensor–surface interface. The charge and organization of the surface monolayer can modulate NA orientation, steric accessibility, and hydration layer dynamics, which collectively influence substrate recognition and catalytic turnover. Such interface effects may either amplify or diminish the apparent differences in substrate specificity among NAs.[44,47] These observations are aligned with our recent findings that surface properties exert a profound impact on enzyme kinetics.[34]

The above results show that the sialoside-based EIS sensing platform possesses several features that are extremely valuable for the development of the VCNA biosensor. First, the unique enzymatic interaction that takes place on the sialoside anchored **AuE**s proved responsive even in complex media derived from two relevant food related samples. Second, the sensor proved relevant even at a pH that is not optimized for the specific enzyme. Third, the contribution of intrinsic enzymatic features towards the different sialosides provides a sensing interface that enables robust discrimination between various NA types. This can be achieved by employing an array of glycans with controlled molecular modifications, which provide unique fingerprints associated with the NAs.

Conclusions

VCNA biosensing at optimal and biorelevant conditions using a sialoside-based electrochemical platform was demonstrated. VCNA exhibits a unique activity profile towards sialosides, differentiating it from other neuraminidases. The biosensing platform demonstrated robust performance in cell growth media and milk, indicating that detection of this biomarker is possible even under non-optimized conditions. Furthermore, while pH influences VCNA activity, it does not completely inhibit the electrochemical response associated with the enzymatic reaction. The developed sialoside-functionalized impedimetric biosensor extends beyond single-substrate detection, offering a robust proof of concept for a multiplexed enzymatic biosensor based on the enzyme's unique fingerprint. This approach leverages an array of distinct sialoside recognition elements on the biosensor surface, allowing for the comprehensive characterization of neuraminidase activity. By individually monitoring the impedimetric response for each sialoside upon exposure to *Vibrio cholerae* neuraminidase, a unique enzymatic fingerprint is generated. This differential activity profile across a panel of sialosides is critical, as it enables the discrimination of VCNA from other neuraminidases that exhibit different substrate specificities.

This multi-sialoside platform thus provides a high-resolution enzymatic signature, reflecting the specific interactions between VCNA and the various immobilized sialosides. The ability to resolve such distinct activity patterns through this multiplexed impedimetric analysis offers significant potential for highly selective pathogen identification and characterization. The applicability demonstrated suggests that further development can yield a robust tool for real-time *Vibrio cholerae* sensing in food chain systems and bioreactors.

Author contributions

H. O. conceived the idea, designed the experiments, conducted experiments, analyzed the results, and wrote the manuscript. I. A. conceived the idea, designed the experiments, analyzed the results, and wrote the manuscript. R. K., S. Y. and M. H. conceived the idea, designed the experiments, supervised the work, and wrote the manuscript.

Conflicts of interest

There are no conflicts to declare.

Data availability

The data supporting this article have been included as part of the supplementary information (SI). Surface characterization using XPS analysis, polarization modulation reflection absorbance infra-red spectroscopy and coverage calculation as well as Nyquist plots can be found in the SI. Supplementary information is available. See DOI: **https://doi.org/10.1039/d5ma00993f**.

Acknowledgements

References

1 A. Jutla, E. Whitcombe, N. Hasan, B. Haley, A. Akanda, A. Huq, M. Alam, R. B. Sack and R. Colwell, *Am. Soc. Trop. Med. Hyg.*, 2013, **89**, 597–607.
2 World Health Organization = Organisation mondiale de la Santé, *Weekly Epidemiological Record*, 2022, **97**, 453–464.
3 A. Aiyar and P. Pingali, *Food Secur.*, 2020, **12**, 749–756.

4 F. Cecchini, L. Fajs, S. Cosnier and R. S. Marks, *TrAC, Trends Anal. Chem.*, 2016, **79**, 199–209.

5 S. Chakraborty, J. Khanam, Y. Takeda and G. B. Nair, *Trans. R. Soc. Trop. Med. Hyg.*, 1999, **93**, 527–528.

6 M. H. Dick, M. Guillerm, F. Moussy and C. L. Chaignat, *PLoS Neglected Trop. Dis.*, 2012, **6**, e1845.

7 B. A. Muzembo, K. Kitahara, A. Debnath, K. Okamoto and S. I. Miyoshi, *Clin. Microbiol. Infect.*, 2022, **28**, 155–162.

8 D. Rocha-Grandal, M. López and A. Garrido-Maestu, *Food Control*, 2025, **168**, 110965.

9 D. A. Negrón, S. Trivedi, N. Tolli, D. Ashford, G. Melton, S. Guertin, K. Jennings, B. D. Necciai, S. Sozhamannan and B. W. Abramson, *BMC Bioinf.*, 2024, **25**, 384.

10 A. Varki, *Nature*, 2007, **446**, 1023.

11 R. Schauer, *Glycoconjugate J.*, 2000, **17**, 485–499.

12 T. Angata and A. Varki, *Chem. Rev.*, 2002, **102**, 439–469.

13 T. K. Altheide, T. Hayakawa, T. S. Mikkelsen, S. Diaz, N. Varki and A. Varki, *J. Biol. Chem.*, 2006, **281**, 25689–25702.

14 E. R. Vimr, K. A. Kalivoda, E. L. Deszo and S. M. Steenbergen, *Microbiol. Mol. Biol. Rev.*, 2004, **68**, 132–153.

15 B. J. Moncla, P. Braham and S. L. Hillier, *J. Clin. Microbiol.*, 1990, **28**, 422–425.

16 S. Kim, D. B. Oh, H. A. Kang and O. Kwon, *Appl. Microbiol. Biotechnol.*, 2011, **91**, 1–15.

17 J. E. Galen, J. M. Ketley, A. Fasano, S. H. Richardson, S. S. Wasserman and J. B. Kaper, *Infect. Immun.*, 1991, **60**, 406–415.

18 S. Manco, F. Hernon, H. Yesilkaya, J. C. Paton, P. W. Andrew and A. Kadioglu, *Infect. Immun.*, 2006, **74**, 4014–4020.

19 I. M. Privalova and A. Y. Khorlin, *Bull. Acad. Sci. USSR, Div. Chem. Sci.*, 1969, **18**, 2614–2619.

20 B. M. Marathe, V. Lévêque, K. Klumpp, R. G. Webster and E. A. Govorkova, *PLoS One*, 2013, **8**, e71401.

21 D. P. Nayak and U. Reichl, *J. Virol. Methods*, 2004, **122**, 9–15.

22 R. C. Buxton, B. Edwards, R. R. Juo, J. C. Voyta, M. Tisdale and R. C. Bethell, *Anal. Biochem.*, 2000, **280**, 291–300.

23 J. Kongkamnerd, A. Milani, G. Cattoli, C. Terregino, I. Capua, L. Beneduce, A. Gallotta, P. Pengo, G. Fassina, O. Monthakantirat, K. Umehara, W. De-Eknamkul and S. Miertus, *J. Biomol. Screening*, 2011, **16**, 755–764.

24 L. Warren, *J. Biol. Chem.*, 1959, **234**, 1971–1975.

25 M. C. Eichelberger, L. Couzens, Y. Gao, M. Levine, J. Katz, R. Wagner, C. I. Thompson, K. Höschler, K. Laurie, T. Bai, O. G. Engelhardt and J. Woodi, *Vaccine*, 2016, **34**, 458–465.

26 M. Prevato, R. Cozzi, A. Pezzicoli, A. R. Taddei, I. Ferlenghi, A. Nandi, E. Montomoli, E. C. Settembre, S. Bertholet, A. Bonci and F. Legay, *PLoS One*, 2015, **10**, 1–14.

27 L. Couzens, J. Gao, K. Westgeest, M. Sandbulte, V. Lugovtsev, R. Fouchier and M. Eichelberger, *J. Virol. Methods*, 2014, **210**, 7–14.

28 I. Kosik and J. W. Yewdell, *Virology*, 2017, **500**, 178–183.

29 A. L. Furst and M. B. Francis, *Chem. Rev.*, 2019, **119**, 700–726.

30 E. Snir, J. Joore, P. Timmerman and S. Yitzchaik, *Langmuir*, 2011, **27**, 11212–11221.

31 S. Yitzchaik, R. Gutierrez, G. Cuniberti and R. Yerushalmi, *Langmuir*, 2018, **34**, 14103–14123.

32 T. Balkenhohl and F. Lisdat, *Analyst*, 2007, **132**, 314–322.

33 D. Butler, N. Goel, L. Goodnight, S. Tadigadapa and A. Ebrahimi, *Biosens. Bioelectron.*, 2019, **129**, 269–276.

34 E. Mervinetsky, I. Alshanski, Y. Hamo, L. M. Sandonas, A. Dianat, J. Buchwald, R. Gutierrez, G. Cuniberti, M. Hurevich and S. Yitzchaik, *Sci. Rep.*, 2017, **7**, 9498.

35 E. Tønning, S. Sapelnikova, J. Christensen, C. Carlsson, M. Winther-Nielsen, E. Dock, R. Solna, P. Skladal, L. Nørgaard, T. Ruzgas and J. Emnéus, *Biosens. Bioelectron.*, 2005, **21**, 608–617.

36 F. Lisdat and D. Schäfer, *Anal. Bioanal. Chem.*, 2008, **391**, 1555–1567.

37 L. Fan, G. Zhao, H. Shi, M. Liu and Z. Li, *Biosens. Bioelectron.*, 2013, **43**, 12–18.

38 L. F. E. Huerta-Nuñez, G. Gutierrez-Iglesias, A. Martinez-Cuazitl, M. M. Mata-Miranda, V. D. Alvarez-Jiménez, V. Sánchez-Monroy, A. Golberg and C. A. González-Díaz, *Sci. Rep.*, 2019, **9**, 6419.

39 I. Alshanski, S. Toraskar, D. Gordon-Levitan, M. Massetti, P. Jain, L. Vaccaro, R. Kikkeri, M. Hurevich and S. Yitzchaik, *Langmuir*, 2024, **40**, 7471–7478.

40 E. Snir, E. Amit, A. Friedler and S. Yitzchaik, *Biopolymers*, 2015, **104**, 515–520.

41 A. Sharma, G. Istamboulie, A. Hayat, G. Catanante, S. Bhand and J. L. Marty, *Sens. Actuators, B*, 2017, **245**, 507–515.

42 B. Martín-Fernández, M.-P. C. Lorena, S.-P. L. Marta, de-los-S.-Á. Noemí and B. López-Ruiz, *Crit. Rev. Food Sci. Nutr.*, 2017, **57**, 2758–2774.

43 E. P. Randviir and C. E. Banks, *Anal. Methods*, 2022, **14**, 4602–4624.

44 I. Alshanski, S. Toraskar, A. Shitrit, D. Gordon-Levitan, P. Jain, R. Kikkeri, M. Hurevich and S. Yitzchaik, *ACS Chem. Biol.*, 2023, **18**, 605–614.

45 T. Matsubara, M. Ujie, T. Yamamoto, M. Akahori, Y. Einaga and T. Sato, *Proc. Natl. Acad. Sci. U. S. A.*, 2016, **113**, 8981–8984.

46 B. Wicklein, M. Á. M. Del Burgo, M. Yuste, E. Carregal-Romero, A. Llobera, M. Darder, P. Aranda, J. Ortín, G. Del Real, C. Fernández-Sánchez and E. Ruiz-Hitzky, *Adv. Funct. Mater.*, 2013, **23**, 254–262.

47 I. Alshanski, A. Shitrit, Y. Sukhran, C. Unverzagt, M. Hurevich and S. Yitzchaik, *Langmuir*, 2022, **38**, 849–855.

48 I. Alshanski, Y. Sukhran, E. Mervinetsky, C. Unverzagt, S. Yitzchaik and M. Hurevich, *Biosens. Bioelectron.*, 2021, **172**, 112762.

49 M. J. Russo, M. Han, P. E. Desroches, C. S. Manasa, J. Dennaoui, A. F. Quigley, R. M. I. Kapsa, S. E. Moulton, R. M. Guijt, G. W. Greene and S. M. Silva, *ACS Sens.*, 2021, **6**, 1482–1507.

50 C. D. Owen, L. E. Tailford, S. Monaco, T. Šuligoj, L. Vaux, R. Lallement, Z. Khedri, H. Yu, K. Lecointe, J. Walshaw, S. Tribolo, M. Horrex, A. Bell, X. Chen, G. L. Taylor, A. Varki, J. Angulo and N. Juge, *Nat. Commun.*, 2017, **8**, 2196.

51 A. B. Boraston, E. Ficko-Blean and M. Healey, *Biochemistry*, 2007, **46**, 11352–11360.

52 I. Moustafa, H. Connaris, M. Taylor, V. Zaitsev, J. C. Wilson, M. J. Kiefel, M. Von Itzstein and G. Taylor, *J. Biol. Chem.*, 2004, **279**, 40819–40826.

53 I. Alshanski, S. Toraskar, K. Mor, F. Daligault, P. Jain, C. Grandjean, R. Kikkeri, M. Hurevich and S. Yitzchaik, *Langmuir*, 2024, **40**, 22152–22158.